Planning for Steerable Bevel-tip Needle Insertion Through 2D Soft Tissue with Obstacles*

Ron Alterovitz and Ken Goldberg
Department of Industrial Engineering and Operations Research
University of California, Berkeley
Berkeley, CA 94720-1777, USA
{ron,goldberg}@ieor.berkeley.edu

Allison Okamura
Department of Mechanical Engineering
The Johns Hopkins University
Baltimore, MD 21218, USA
aokamura@jhu.edu

***Abstract*— Medical procedures such as seed implantation, biopsies, and treatment injections require inserting a needle to a specific target location inside the human body. Flexible needles with bevel tips are known to bend when inserted into soft tissues and can be inserted to targets unreachable by rigid symmetric-tip needles. Planning for such procedures is difficult because needle insertion causes soft tissues to displace and deform. In this paper, we develop a 2D planning algorithm for insertion of highly flexible bevel-tip needles into tissues with obstacles. Given an initial needle insertion plan specifying location, orientation, bevel rotation, and insertion distance, the planner combines soft tissue modeling and numerical optimization to generate a needle insertion plan that compensates for simulated tissue deformations, locally avoids polygonal obstacles, and minimizes needle insertion distance. Soft tissue deformations are simulated using a finite element formulation that models the effects of needle tip and frictional forces using a 2D mesh. The planning problem is formulated as a constrained nonlinear optimization problem which is locally minimized using a penalty method that converts the formulation to a sequence of unconstrained optimization problems. We apply the planner to bevel-right and bevel-left needles and generate plans for targets that are unreachable by rigid needles.**

***Index Terms*— steerable needle, medical robotics, surgery, catheter, biopsy, brachytherapy, planning.**

I. Introduction

Needle insertion is a critical step in many diagnostic and therapeutic medical procedures, including biopsy to obtain a specific tissue sample for testing, drug treatment injections for anesthesia, or radioactive seed implantation for brachytherapy cancer treatment. In these procedures, a needle must be guided to a specific target in soft tissue. In this paper we consider highly flexible bevel-tip needles that can be steered around obstacles by taking advantage of needle bending and the asymmetric force applied by the needle tip to the tissue. These steerable needles are capable of reaching targets inaccessible by rigid needles.

The success of medical needle insertion procedures often depends on the accuracy with which the needle can be guided to a specific target in soft tissue. Unfortunately, inserting and retracting needles causes the surrounding soft tissues to displace and deform: ignoring these deformations can lead to significant errors between needle tip and target positions. In permanent seed brachytherapy, physicians use slightly flexible needles to permanently implant radioactive seeds inside the prostate that irradiate surrounding tissue over several months. Successful treatment depends on the accurate placement of radioactive seeds within the prostate gland [6], [17]. However, tissue deformations and needle bending lead to significant errors in seed implantation locations [18], [17], [21], [1], [2].

Fast and accurate computer simulations of needle insertion procedures can facilitate physician training and assist in pre-operative planning and optimization. In this paper we develop a 2D simulation and planner for steerable bevel-tip

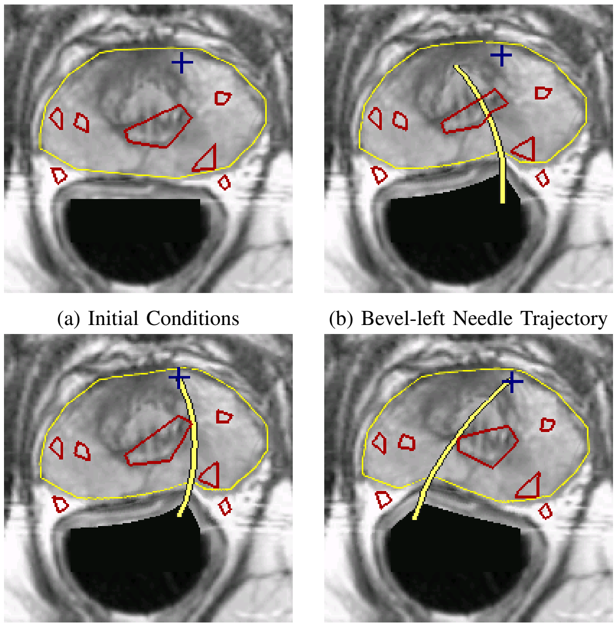

(a) Initial Conditions (b) Bevel-left Needle Trajectory (c) Bevel-left Plan (b) Bevel-right Plan

Fig. 1. In this example based on an MR image of the prostate [13], a biopsy needle attached to a rigid rectal probe (black half-circle) is inserted into the prostate (outlined in yellow) using simulation. Obstacles (red polygons) and the target (blue cross) are overlaid on the image. The target is not accessible from the rigid probe by a straight line path without intersecting obstacles. However, bevel-tip needles bend as they are inserted into soft tissue (b). Our planner computes a locally optimal bevel-left needle insertion plan that reaches the target, avoids obstacles, and minimizes insertion distance (c). Using different initial conditions, our planner generates a plan for a bevel-right needle (d). Due to tissue deformation, the needle paths do not have constant curvature.

*This work was supported in part by the National Institutes of Health under grant R21 EB003452 and a National Science Foundation Graduate Research Fellowship.

needle insertion. The simulation achieves video frame rates and can be used to interactively demonstrate to physicians the effect of tissue deformations during needle insertion. Our simulation approximates soft tissues as linearly elastic materials and uses a 2D finite element model to compute tissue deformations due to tip and friction forces applied by the steerable needle.

In this paper we develop a planner that uses the simulation to compute a locally optimal needle insertion location and orientation to compensate for tissue deformations and reach the target while avoiding obstacles defined by polygons in the soft tissue. In a medical setting, obstacles represent tissues that cannot be cut by the needle, such as bone, or sensitive tissues that should not be damaged, such as nerves or arteries. Our planner considers 4 degrees of freedom: initial location, initial orientation, binary bevel rotation, and insertion distance. We compute locally optimal values for these variables so that the needle in simulation reaches the target and avoids polygonal obstacles while minimizing insertion distance so less tissue is damaged by the needle. Even in situations where real-time imaging such as ultrasound or interventional MRI is available, preplanning is valuable to set the needle initial location and orientation and compute a desired trajectory that minimizes tissue damage.

II. Related Work

Needle insertion simulation requires estimating biomechanical deformations of soft tissue when forces are applied. The history of offline animation and real-time simulation of deformable objects is summarized in [10]. The feasibility and potential of the finite element method (FEM), which is based on the equations of continuum mechanics, for animation was demonstrated by Terzopolous et al. [23]. Real-time visual performance for surgery simulation of the human liver using FEM was achieved by Cotin et al., although the required preprocessing step took 8 hours on a standard PC [5]. They modeled tissue as a linearly elastic material and allowed only small quasi-static deformations. Our soft tissue simulator also models linear elastic materials but relaxes the quasi-static assumption and simulates dynamic deformations, as formulated by Zhuang [27] and Picinbono et al. [16]. Setting accurate parameters for tissue properties is important for realistic simulation. Krouskop et al. estimated the elastic modulus for prostate and breast tissue using ultrasonic elastography [14].

Earlier work on interactive simulation of needle insertion assumed only 2D planar deformations and a thin rigid needle with a symmetric tip [7], [3], [1]. Physical measurements of forces exerted during needle insertion were measured by Kataoka et al., who separately measured tip and frictional forces during needle insertion into a canine prostate [12]. Planning optimal insertion location and insertion distance to compensate for tissue deformations has been addressed for 2D rigid needles [2].

DiMaio and Salcudean modeled a flexible symmetric-tip needle with 2D triangular elements and used a nonlinear finite element method to compute the needle's deformation [8]. Key nodes from the needle mesh were embedded in a tissue mesh whose deformations were computed using a linear quasi-static finite element method.

Our interactive simulation relaxes both the needle rigidity and symmetric-tip assumptions by modeling steerable bevel-tip needles. Okamura et al. are studying paths of flexible bevel-tip needles during insertion [24]. O'Leary et al. showed that needles with bevel tips bend more than symmetric-tip needles [15]. Webster et al. developed thin highly flexible bevel-tip needles using Nitinol and experimentally tested them in very stiff tissue phantoms [24]. The needles followed constant-curvature paths in a plane when bevel rotation was fixed during needle insertion.

Webster el al. [24] developed a nonholonomic model for steering flexible bevel-tip needles in rigid tissues. The nonholonomic model, a generalization of a 3 degree-of-freedom bicycle model, was experimentally validated using a very stiff tissue phantom. Recent advances by Zhou and Chirikjian in nonholonomic path planning include stochastic model-based motion planning to compensate for noise bias [26] and probabilistic models of dead-reckoning error in nonholonomic robots [25].

Past work has addressed steering symmetric-tip needles in 2D deformable tissue that have 3 degrees of freedom: translating the needle base perpendicular to the insertion direction, rotating the the needle base along an axis perpendicular to the plane of the tissue, and translation along the needle insertion axis [8], [11]. DiMaio and Salcudean compute and invert a Jacobian matrix to translate and orient the base to avoid point obstacles with oval-shaped potential fields. Glozman and Shoham approximate the tissue using springs and also use an inverse kinematics approach to translate and orient the base every time step. In our work, we address bevel-tip steerable needles that have 2 degrees of freedom during insertion: rotation about the insertion axis and translation along the insertion axis. We are not aware of past work that has explicitly considered the effect of tissue deformations on this type of steerable needle.

Medical needle insertion procedures may benefit from the more precise control of needle position and velocity made possible through robotic surgical assistants. A survey of recent advances in medical robotics was written by Taylor and Stoianovici [22]. Dedicated hardware for prostate biopsy needle insertion procedures that can be integrated with transrectal ultrasound imaging is being developed by Fichtinger et al. [9], [19].

III. Simulation of Bevel-tip Needle Insertion

A bevel-tip needle, unlike a symmetric-tip needle, will cut tissue at an angle, as shown in Fig. 2. Since the needle cuts at an angle away from the direction of insertion, the needle may bend in the direction of the bevel.

Our simulation models forces exerted by the needle on the soft tissue, including the cutting force at the needle tip and friction forces along the needle shaft. We assume needle bending forces are negligible compared to the elastic forces applied by the soft tissue to the needle.

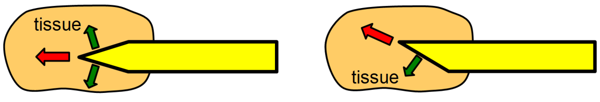

(a) Symmetric tip (b) Bevel tip

Fig. 2. A symmetric-tip needle exerts forces on the tissue equally in all directions, so it cuts tissue in the direction that the tip is moving. A bevel-tip needle exerts forces asymmetrically and cuts tissue at an offset angle depending on the tissue properties and bevel angle.

We first describe our soft tissue model and method for computing soft tissue deformations due to forces applied by the needle. We then describe our model for cutting and frictional forces applied by the needle during insertion.

A. Soft Tissue Model

We specify the anatomy geometry (i.e. the prostate and surrounding tissues) using a finite element mesh. The geometric input is a 2D slice of tissue with tissue types segmented by polygons. Based on the polygonal segmentation boundaries, we automatically generate a finite element mesh G composed of n nodes and m triangular elements in a regular right triangle mesh or using the constrained Delaunay triangulation software program Triangle [20], which generates meshes that conform to the segmented tissue type polygons.

The model must also include the tissue material properties and boundary conditions for the finite element mesh. In our current implementation, we approximate soft tissues as linearly elastic, homogeneous, isotropic materials. For each segmented tissue type, the model requires as input the tissue material properties (the Young's modulus, Poisson ratio, and density). We set values for these parameters as described in past work [2]. Each element in the mesh may be assigned unique material properties, which allows for the simulation of multiple tissue types in one mesh. Mesh nodes defining elements inside bones are constrained to be fixed. A boundary condition of either free or fixed must be specified for each node on the perimeter of the finite element mesh.

The complete tissue model M specifies the finite element mesh G, material properties, and boundary conditions. We assume the tissue in M is initially at equilibrium and ignore external forces not applied by the needle. We do not model physiological changes such as edema (tissue swelling), periodic tissue motion due to breathing or heart beat, or slip between tissue type boundaries.

B. Computing Soft Tissue Deformations

The *reference mesh* G defines the geometry of the tissues, with each node i having coordinate $\mathbf{x}_i$ in the material frame, which specifies the geometry of the tissue without any deformation. Forces resulting from needle insertion cause the tissue to deform. The deformation is defined by a displacement $\mathbf{u}_i$ for each node i in mesh G. The *deformed mesh* G' is constructed in the world frame using the displaced node coordinate $\mathbf{x}_i + \mathbf{u}_i$ for each node i. At each time step we compute the acceleration of each node i, which includes acceleration due to elastic forces computed using a linear finite element method and acceleration due to the external force $\mathbf{f}_i$ exerted by the needle. We use explicit Euler time integration to integrate velocity and displacement for each free node for each time step. Time steps have duration $h = 0.01$ seconds.

C. Needle Insertion Model

Without loss of generality, we set the coordinate axes of the world frame so that the default needle insertion axis is along the positive z-axis. The y-axis corresponds to the initial location degree of freedom. The needle tip is initially located at a base coordinate $\mathbf{p}_0 = (y_0, z_0)$. The initial orientation of the needle is specified using θ, as shown in Fig. 3. For simulation stability, we constrain θ between $-45°$ and $45°$. The needle tip rotation is either bevel-right ($0°$) or bevel-left ($180°$). We assume the needle tip rotation is held constant during insertion.

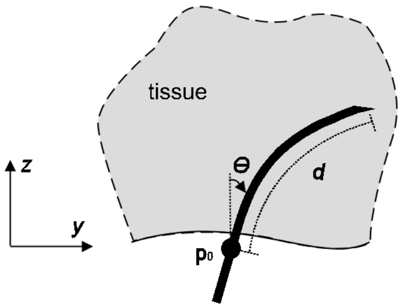

Fig. 3. Slice of soft tissue in the yz plane. The bevel-tip needle is initially at the base coordinate $\mathbf{p}_0$ with orientation θ. It is inserted a distance d, causing the surrounding soft tissue to deform.

The needle is inserted along the z-axis until it comes in contact with tissue. We assume the flexible needle is supported so that it does not bend outside the tissue. Once the needle has entered the tissue, it will bend in the direction of the bevel-tip. The distance the needle has been inserted from the base coordinate is d, as shown in Fig. 3. We parameterize the needle by s where $s = 0$ corresponds the needle base and $s = d$ corresponds to the needle tip. Let $\mathbf{p}_s$ denote the material frame coordinate of the point along the needle a distance s from the base.

Simulation of needle insertion requires a needle model N that specifies needle properties, including insertion velocity v, cutting force (force at the needle tip required to cut tissue), and the static and kinetic coefficients of friction between the tissue and needle.

We model the needle by the chain of nodes in the tissue mesh along the needle path. These nodes define needle line segment elements that correspond to edges in the tissue mesh. This representation of the needle facilitates real-time interactive performance since no expensive collision detection between the needle and soft tissue is required. At each simulation time step, the needle exerts force on the tissue at the needle tip, where the needle is displacing and cutting the tissue, and frictional forces are applied along the needle shaft.

We apply needle forces as boundary conditions on elements in the reference mesh. Since the needle may be inserted at any location, it is usually necessary to modify the reference mesh in real-time to ensure that element boundaries are present where the tip and friction forces must be applied. To apply the tip force, a node is maintained at the needle tip location during insertion. To apply the friction forces, a list of nodes along the needle shaft is maintained.

Highly flexible bevel-tip needles tested in tissue phantoms by Webster et al. [24] were experimentally shown to follow a constant-curvature path when the bevel rotation was fixed during needle insertion. In our simulation, setting simulation parameters to the limiting case of highly stiff tissue, zero tissue cutting force, and zero friction allows us to replicate this constant curvature path. In other cases, the needle path through deformed tissue may not be of constant curvature.

D. Simulating Cutting at the Needle Tip

During each simulation time step, the needle tip moves a distance vh in the world frame, where v is the needle insertion velocity and h is the time step duration. The simulation must maintain element edges along the needle path, which requires mesh modification as the needle cuts through the tissue.

The simulation constrains a node to be located at the needle tip. The current needle tip node is labeled n_{tip} and the needle is pointed in direction $\mathbf{q}$. The needle will cut tissue a small distance d_{cut} along the vector $\mathbf{r}$ in the world frame, where $\mathbf{r}$ is deflected from $\mathbf{q}$ by an angle θ_d, as shown in Fig. 4. If the force at the needle tip along $\mathbf{r}$ is greater than a threshold f_{cut} based on needle and tissue properties, then the needle will cut through the tissue. Cutting is represented in the material mesh by moving the needle tip node n_{tip} by the distance d_{cut} transformed to the material frame. If no tissue deformation occurs, this method guarantees the needle will cut a path of constant curvature whose radius of curvature is a function of the deflection angle θ_d. When tissue deformations do occur at the needle tip, the path will be of constant curvature locally but will deviate from constant curvature globally depending on the magnitude of the deformations.

As the needle tip cuts through the mesh, it will be necessary to change the needle tip node. If the needle tip node is too close to the opposite triangle edge e, the tip node is moved back along the shaft and a new tip node, the closest node along edge e, is selected as the new tip node and moved to the new tip location in the material frame. The simulator maintains a list of all nodes along the needle shaft, including the tip node.

E. Simulating Friction Along the Needle Shaft

A stick-slip friction model is used to simulate friction between the needle and the soft tissue. Nodes along the needle shaft carry friction state information; they are either attached to the needle (in the static friction state) or allowed to slide along the needle shaft (in the dynamic friction state).

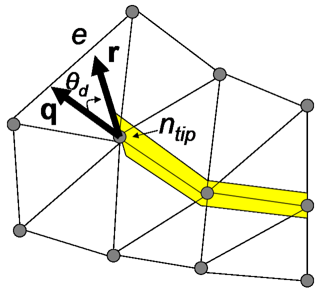

Fig. 4. The tissue mesh is modified so edge boundaries are formed along the path of needle insertion. A subset of the tissue mesh, centered at needle tip node n_{tip}, is shown. The straight line path of the needle is shown by vector $\mathbf{q}$. Because of the bevel-tip, the needle cuts tissue in direction $\mathbf{r}$, which is deflected from $\mathbf{q}$ by θ_d degrees.

When a node enters the static friction state, its distance from the needle tip along the shaft is computed. For each time step where the node remains in the static friction state, its position is modified by moving it tangent to the needle so that its distance from the tip along the needle shaft is held constant. A node moves from the static to the dynamic friction state when the force required to displace the node along the needle shaft exceeds a slip force parameter f_{s-max}.

When a node is in the dynamic friction state, a dissipative force is applied along the needle tangent in the direction of needle insertion. A node moves from the dynamic to the static friction state when the relative velocity of the needle to the tissue at the node is close to zero.

F. Simulation Results

We demonstrate our simulation results in 2 cases: rigid tissue and deformable tissue. In both cases we simulate the insertion of a bevel-tip needle into a square of soft tissue constrained as fixed on 3 sides. In the first case, we consider tissue that is stiff relative to the needle and a sharp frictionless needle that cuts the tissue with zero cutting force. As shown in Fig 5.(a), the simulated needle follows a path of constant curvature, which is the behavior experimentally verified by Webster et al. [24]. In the second case, we insert a needle into a deformable soft tissue mesh with positive cutting force and friction coefficients. As shown in Fig. 5(b), the mesh deforms and the needle follows a curved path in the direction of the bevel-tip. Although the tip locally follows a path of constant curvature as explained in Section III-D, the global path is not of constant curvature. Past experiments have demonstrated the effect of tissue deformations due to rigid needle insertion [7], [1]. We plan to develop experiments to test the bending behavior of flexible bevel-tip needles in deformable tissues to more accurately set parameters for our model in future work.

Our simulator was implemented in C++ using OpenGL for visualization. It achieved an average frame rate of approximately 100 frames per second on a 1.6GHz Pentium

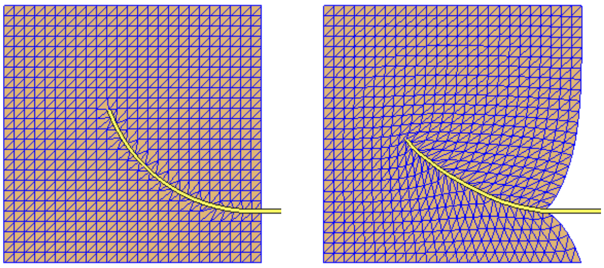

(a) Rigid Tissue (b) Deformable Tissue

Fig. 5. We simulate the insertion of a bevel-tip needle into a square of tissue constrained as fixed on 3 sides. When the tissue is stiff relative to the needle and a sharp frictionless needle is used that cuts tissue with zero cutting force, the needle follows a path of constant curvature (a). For soft tissue and needles with positive cutting and friction forces, the needle bends in the deformable tissue (b).

M computer for the example above using a mesh composed of 1250 triangular elements. Computation time per frame increases linearly as the number of nodes along the needle shaft increases.

IV. Planning

A needle insertion plan is defined by $X = (y_0, \theta, b, d)$ where $y_0 \in \mathbb{R}$ is the insertion location, $\theta \in [-90°, 90°]$ is the insertion angle, $b \in \{0°, 180°\}$ is the bevel rotation, and $d \in \mathbb{R}^+$ is the distance the needle will be inserted. Obstacles are defined as nonoverlapping polygons in a set O. The target is defined as a point $\mathbf{t}$ in the material frame of the soft tissue mesh. A plan X is feasible if the needle tip is within $\epsilon_t > 0$ of the target and the needle path in deformable tissue does not intersect any obstacle. The goal of needle insertion planning is to generate a feasible plan X that minimizes d.

A. Problem Formulation

The simulation of needle insertion described in Section III takes parameters X for the initial conditions and needle insertion distance, M for the soft tissue model, and N for the needle model and outputs the coordinates $\mathbf{p}_s$ for $s \in [0, d]$ that the needle will follow in the material frame.

$$\mathbf{p}_s = \text{NeedleSim}(X, M, N), s \in [0, d]$$

The variables of plan X are constrained by application specific limits y_{min}, y_{max}, θ_{min}, θ_{max}, and d_{max}. These parameters cannot exceed than the limits of the simulation, such as the angle requirements in Section III-C. In the biopsy example in Fig. 1, d_{max} is the maximum length of the needle and $y_{max} - y_{min}$ defines the width of the rectal probe. The limit constraints are defined as follows.

$$y_{min} \leq y_0 \leq y_{max}$$
$$\theta_{min} \leq \theta \leq \theta_{max}$$
$$0 \leq d \leq d_{max}$$

Furthermore, the needle tip coordinate $\mathbf{p}_d$ in a feasible solution must be within Euclidean distance ϵ_t of the target $\mathbf{t}$.

$$\|\mathbf{p}_d - \mathbf{t}\| \leq \epsilon_t$$

In the presence of a nonempty set of polygonal obstacles O, we require that the needle path in a feasible solution does not intersect an obstacle. Let c_s be the distance from $\mathbf{p}_s$ to the closest point on the closest obstacle $o \in O$ and let the sign of c_s be negative if $\mathbf{p}_s$ is inside obstacle o and positive otherwise. We require $c_s \geq \epsilon_o$ for some given tolerance $\epsilon_o \geq 0$ for all points s along the needle shaft. We formulate this constraint as

$$\int_0^d \max\{-c_s + \epsilon_o, 0\} ds \leq 0.$$

We can quickly compute this integral numerically using points sampled along the needle path.

We summarize the problem formulation for variable $X = (y_0, \theta, b, d)$ given target coordinate $\mathbf{t}$, polygonal obstacles O, tolerances ϵ_t and ϵ_o, tissue model parameters M, needle model parameters N, and variable limits y_{min}, y_{max}, θ_{min}, θ_{max}, and d_{max}.

$$\begin{aligned}
&\min f(X) = d \\
&\text{Subject to:} \\
&\quad \|\mathbf{p}_d - \mathbf{t}\| \leq \epsilon_t \\
&\quad \textstyle\int_0^d \max\{-c_s + \epsilon_o, 0\} ds \leq 0 \\
&\quad y_{min} \leq y_0 \leq y_{max} \\
&\quad \theta_{min} \leq \theta \leq \theta_{max} \\
&\quad 0 \leq d \leq d_{max}
\end{aligned}$$

The values of $\mathbf{p}_s$ for $s \in [0, d]$ are computed by executing the simulator NeedleSim(X, M, N). The obstacle distances c_s for $s \in [0, d]$ are computed using $\mathbf{p}_s$ and the set of obstacles O.

B. Optimization Method

To reduce the complexity of the optimization, we reduce the number of variables in X from 4 to 2. Given a plan X, we can find the optimal insertion distance d by executing the simulation to insertion distance d_{max} and identifying the point $\mathbf{p}_s$ along the needle path that minimizes the distance to the target $\mathbf{t}$. Hence, d does not need to be explicitly treated as a variable since its value is implied by the other variables in X. Furthermore, variable b in X is binary since it represents the bevel-right or bevel-left needle rotation state. We optimize X separately for the bevel-right and bevel-left states.

We solve for a locally optimal solution X^* using a penalty method. Penalty methods, originally developed in the 1950's and 1960's, solve a constrained nonlinear optimization problem by converting it to a series of unconstrained nonlinear optimization problems [4]. Given the constrained optimization problem $\min f(\mathbf{x})$ subject to $g(\mathbf{x}) \leq 0$, we can write the unconstrained problem $\min(f(\mathbf{x}) + \mu \max\{0, g(\mathbf{x})\}^2)$ for some large $\mu > 0$. Penalty methods generate a series of unconstrained optimization problems as $\mu \to \infty$. Each unconstrained optimization problem can be solved using Gradient Descent or variants of Newton's Method. For convex nonlinear problems, the method will generate points that converge arbitrarily close to the global optimal solution [4]. For nonconvex problems, the method can only converge to a local optimal solution.

For steerable needle insertion planning, we convert the target and obstacle constraints to penalty functions to define a new nonlinear nonconvex optimization problem.

$$\min \hat{f}(X) = d + \mu \left(\max\{\|\mathbf{p}_d - \mathbf{t}\| - \epsilon_t, 0\}\right)^2 + \mu \left(\int_0^d \max\{-c_s + \epsilon_o, 0\} ds\right)^2$$

Subject to:

$$y_{min} \leq y_0 \leq y_{max}$$
$$\theta_{min} \leq \theta \leq \theta_{max}$$
$$0 \leq d \leq d_{max}$$

Evaluating the objective function $\hat{f}(X)$ requires executing the simulator NeedleSim(X, M, N) to compute the needle path $\mathbf{p}_s$ for $s \in [0, d]$ and the obstacles distances c_s. The remaining constraints are the limit constraints that are required for simulation stability and can never be violated.

We use the Gradient Descent algorithm to find a local optimal solution to the unconstrained minimization problem $\min \hat{f}(X)$. The trivial limit constraints are easily enforced at each iteration of the optimization method implementation. We solve a sequence of 4 unconstrained problems, each with 10 Gradient Descent iterations. After each unconstrained problem has been solved, we multiply the penalty factor μ by 10. We plan in the future to determine problem-specific termination criteria for the unconstrained optimization problems and for the penalty method.

The objective function $\hat{f}(X)$ cannot be directly differentiated since the simulator cannot be written as a closed form equation. For the Gradient Descent method, we numerically approximate the derivatives of the objective function with respect to the insertion location y_0 and orientation θ. We compute $d\hat{f}/dy_0$ by translating the needle path by Δy_0 and recomputing $\hat{f}$. Similarly, we compute $d\hat{f}/d\theta$ by rotating the needle path by $\Delta\theta$ about the insertion base coordinate $\mathbf{p}_0$ and recomputing $\hat{f}$. These approximations do not explicitly account for the different deformations that occur when y_0 or θ are modified but were sufficiently accurate for small Δy_0 and $\Delta\theta$ in our results described below.

C. Planner Results

Our planner was implemented in C++ and uses the simulation described in Section III. Results for a medical biopsy example are shown in Fig. 1. The tissue model mesh was composed of 1196 triangular elements and the planner required approximately 5 minutes of computation time on a Pentium M 1.6GHz computer to generate the plans shown in Fig. 1(c) and (d). We demonstrate the results of the planner for another prostate case through a different image plane in Fig. 6.

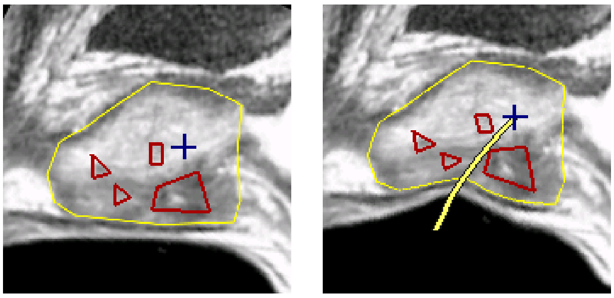

(a) Initial Conditions (b) Bevel-right Plan

Fig. 6. In this example based on an MR image of the sagittal plane of the prostate [13], a biopsy needle is inserted into the prostate (outlined in yellow) (a). The planner computes an initial position, orientation, and insertion distance so the needle reaches the target (blue cross) while avoiding obstacles (red polygons) and compensating for tissue deformations in simulation (b).

V. Conclusion

We describe a needle insertion planning algorithm for steerable bevel-tip needles. The method combines numerical optimization with soft tissue simulation. The simulation, based on a linear finite element method, models the effects of needle tip and frictional forces on soft tissues defined by a 2D mesh. Our planning algorithm computes a locally optimal initial location, orientation, and insertion distance for the needle to compensate for predicted tissue deformations and reach a target while avoiding polygonal obstacles.

The effectiveness of the planner is dependent on the accuracy of the simulation of steerable needle insertion and soft tissue deformations. In future work, we will compare the output of our simulation to new physical experiments, consider a finite set of different needle bevel types, allow bevel rotation during insertion, improve the efficiency of our optimization method, and extend our simulation and planner to 3D.

Acknowledgment

We thank Russ Taylor for introducing us to the problem of needle insertion and James F. O'Brien, John Kurhanewicz, Gabor Fichtinger, Greg Chirikjian, Robert Webster, Tim Salcudean, Simon DiMaio, A. Frank van der Stappen, K. Gopalakrishnan, Dezhen Song, and Michael Yu for their valuable feedback and assistance. We also thank physicians Leonard Shain of CPMC and I-Chow Hsu of UCSF for their feedback on medical aspects of this work.

References

[1] R. Alterovitz, J. Pouliot, R. Taschereau, I.-C. Hsu, and K. Goldberg, "Needle insertion and radioactive seed implantation in human tissues: Simulation and sensitivity analysis," in *Proc. IEEE International Conference on Robotics and Automation (ICRA)*, vol. 2, Sept. 2003, pp. 1793–1799.

[2] ——, "Sensorless planning for medical needle insertion procedures," in *Proc. IEEE/RSJ International Conference on Intelligent Robots and Systems (IROS)*, vol. 3, Oct. 2003, pp. 3337–3343.

[3] ——, "Simulating needle insertion and radioactive seed implantation for prostate brachytherapy," in *Medicine Meets Virtual Reality 11*, J. D. Westwood *et al.*, Eds. IOS Press, Jan. 2003, pp. 19–25.

[4] M. S. Bazaraa, H. D. Sherali, and C. M. Shetty, *Nonlinear Programming: Theory and Algorithms*, 2nd ed. John Wiley & Sons, Inc., 1993.

[5] S. Cotin, H. Delingette, and N. Ayache, "Real-time elastic deformations of soft tissues for surgery simulation," *IEEE Trans. on Visualization and Computer Graphics*, vol. 5, no. 1, 1999.

[6] J. E. Dawson, T. Wu, T. Roy, J. Y. Gy, and H. Kim, "Dose effects of seeds placement deviations from pre-planned positions in ultrasound guided prostate implants," *Radiotherapy and oncology*, vol. 32, no. 2, pp. 268–270, 1994.
[7] S. P. DiMaio and S. E. Salcudean, "Needle insertion modeling and simulation," in *Proc. IEEE International Conference on Robotics and Automation (ICRA)*, May 2002, pp. 2098–2105.
[8] ——, "Needle steering and model-based trajectory planning," in *Medical Image Computing and Computer Assisted Intervention (MICCAI)*, 2003.
[9] G. Fichtinger, T. L. DeWeese, A. Patriciu, A. Tanacs, D. Mazilu, J. H. Anderson, K. Masamune, R. H. Taylor, and D. Stoianovici, "System for robotically assisted prostate biopsy and therapy with intraoperative CT guidance," *Academic Radiology*, vol. 9, no. 1, pp. 60–74, 2002.
[10] S. F. Gibson and B. Mirtich, "A survey of deformable modeling in computer graphics," MERL, TR-97-19, Tech. Rep., 1997.
[11] D. Glozman and M. Shoham, "Flexible needle steering and optimal trajectory planning for percutaneous therapies," to appear in Medical Image Computing and Computer Assisted Intervention (MICCAI), Sept. 2004.
[12] H. Kataoka, T. Washio, K. Chinzei, K. Mizuhara, C. Simone, and A. Okamura, "Measurement of tip and friction force acting on a needle during penetration," in *Medical Image Computing and Computer Assisted Intervention (MICCAI)*, ser. Lecture Notes in Computer Science, T. Dohi and R. Kikinis, Eds., vol. 2488. Springer, 2002, pp. 216–223.
[13] Y. Kim, "Image-based high dose rate (HDR) brachytherapy for prostate cancer," Ph.D. dissertation, UC Berkeley, Dec. 2003.
[14] T. A. Krouskop, T. M. Wheeler, F. Kallel, B. S. Garria, and T. Hall, "Elastic moduli of breast and prostate tissues under compression," *Ultrasonic Imaging*, vol. 20, no. 4, pp. 260–274, Oct. 1998.
[15] M. D. O'Leary, C. Simone, T. Washio, K. Yoshinaka, and A. M. Okamura, "Robotic needle insertion: Effects of friction and needle geometry," in *Proc. IEEE International Conference on Robotics and Automation (ICRA)*, Sept. 2003, pp. 1774–1780.
[16] G. Picinbono, H. Delingette, and N. Ayache, "Nonlinear and anisotropic elastic soft tissue models for medical simulation," *Proc. IEEE International Conference on Robotics and Automation (ICRA)*, pp. 1370–1375, May 2001.
[17] J. Pouliot, R. Taschereau, C. Coté, J. Roy, and D. Tremblay, "Dosimetric aspects of permanent radioactive implants for the treatment of prostate cancer," *Physics in Canada*, vol. 55, no. 2, pp. 61–68, 1999.
[18] P. L. Roberson, V. Narayana, P. L. McShan, R. J. Winfield, and P. W. McLaughlin, "Source placement error for permanent implant of the prostate," *Medical Physics*, vol. 24, pp. 251–257, 1997.
[19] C. Schneider, A. M. Okamura, and G. Fichtinger, "A robotic system for transrectal needle insertion into the prostate with integrated ultrasound," in *Proc. IEEE International Conference on Robotics and Automation (ICRA)*, May 2004, pp. 2085–2091.
[20] J. Shewchuck, "Triangle: A two-dimensional quality mesh generator and delaunay triangulator," Available: http://www-2.cs.cmu.edu/ quake/triangle.html, 2002.
[21] R. Taschereau, J. Roy, and J. Pouliot, "Monte carlo simulations of prostate implants to improve dosimetry and compare planning methods," *Medical Physics*, vol. 26, no. 9, Sept. 1999.
[22] R. H. Taylor and D. Stoianovici, "Medical robotics in computer-integrated surgery," *IEEE Transactions on Robotics and Automation*, vol. 19, no. 5, pp. 765–781, Oct. 2003.
[23] D. Terzopolous, J. Platt, A. Barr, and K. Fleischer, "Elastically deformable models," *Computer Graphics*, vol. 21, no. 4, July 1987.
[24] R. J. Webster III, N. J. Cowan, G. Chirikjian, and A. M. Okamura, "Nonholonomic modeling of needle steering," in *Proc. 9th International Symposium on Experimental Robotics*, June 2004.
[25] Y. Zhou and G. S. Chirikjian, "Probabilistic models of dead-reckoning error in nonholonomic mobile robots," in *Proc. IEEE International Conference on Robotics and Automation (ICRA)*, Sept. 2003, pp. 1594–1599.
[26] ——, "Planning for noise-induced trajectory bias in nonholonomic robots with uncertainty," in *Proc. IEEE International Conference on Robotics and Automation (ICRA)*, Apr. 2004, pp. 4596–4601.
[27] Y. Zhuang, "Real-time simulation of physically realistic global deformations," Ph.D. dissertation, UC Berkeley, 2000.